INTERNATIONAL JOURNAL OF INTEGRATED ENGINEERING
ISSN: 2229-838X e-ISSN: 2600-7916

IJIE

Vol. 16 No. 5 (2024) 46-55
https://publisher.uthm.edu.my/ojs/index.php/ijie

Integrating Numerical Simulation and Experimental Validation to Analyze Temperature Distribution in Friction Stir Welding of Dissimilar Aluminum Alloy

K. Samadhanam Raju[1]*, N. Ramanaiah[1]

[1] *Mechanical Engineering, AU College of Engineering, Andhra University, Visakhapatnam, 530003, INDIA*

*Corresponding Author: samadhanamrajukaranam@gmail.com
DOI: https://doi.org/10.30880/ijie.2024.16.05.005

Article Info

Received: 17 April 2024
Accepted: 20 May 2024
Available online: 1 August 2024

Keywords

Temperature distribution, friction stir welding (FSW), numerical analysis, dissimilar friction stir welding (DFSW), validation

Abstract

This study explores the temperature distribution in Aluminum alloys, specifically AA2024 T351 and AA6351 T6, during friction stir welding (FSW). Utilizing COMSOL Multiphysics software, the research investigates FSW at rotational speeds of 800, 1200, and 1600 rpm, while maintaining a constant welding speed (35 mm/min) and axial force (3 kN). The simulation incorporates temperature-dependent material properties. The findings reveal that the maximum temperature occurs at the upper part of the stir zone for both alloys. Experimental validation demonstrates excellent agreement with the simulated temperature distribution, reaffirming the accuracy of the COMSOL Multiphysics model.

1. Introduction

In the realm of solid-state welding, Friction Stir Welding (FSW) stands out as a pivotal technique, seamlessly joining materials without resorting to melting (Figure 1). Conceived at The Welding Institute (TWI) in 1991, FSW has since found widespread use across diverse industries. This innovative process utilizes a rotating tool that traverses the joint between materials, generating heat and pressure. This dual force softens the materials, enabling their fusion. Notably, FSW is remarkably versatile, adept at welding challenging materials like aluminum, copper, titanium, and steel, particularly valuable for alloys prone to cracking and distortion during traditional welding methods.

FSW's advantages are manifold: it yields high-strength, defect-free welds with minimal distortion and low thermal impact. Additionally, it generates negligible fumes, eliminating the need for shielding gas or flux and promoting environmental friendliness. Its applications span aerospace, automotive, shipbuilding, and railway industries, extending to the production of intricate structures like heat exchangers and cryogenic tanks.

Researchers have delved deep into FSW's complexities, employing advanced simulation techniques. Notably, Song et al. (2003) pioneered a 3-D transient heat transfer FSW model in COMSOL Multiphysics, showcasing the difficulty of measuring temperature near the moving rotational tool. Their study, focused on AA6061-T6 with an H13 tool, revealed a nugget zone temperature of 820K. Others, like Zhang et al. (2009), Padmanaban et al. (2014), Salimi et al. (2014), Vignesh et al. (2016), Maharia et al. (2018), Pamuk et al. (2018), Tayo et al. (2019), Vishwanath et al. (2019), Sevvel et al. (2020), and Lemi et al. (2022), have furthered this research frontier. They explored factors such as tool speed, material properties, and atmospheric conditions, employing numerical simulations in COMSOL and other tools like ABAQUS and ANSYS. Their studies have deepened our understanding of FSW, offering insights crucial for optimizing this revolutionary welding technique.

The field of friction stir welding has seen extensive research on similar and dissimilar materials, exploring various process parameters. However, there is still a gap in understanding the joining of specific alloys and the

influence of process variables on temperature distribution, critical for enhancing weld quality tailored for diverse applications.

The primary objective of this study is to delve into unexplored territories by simulating temperature distribution using COMSOL Multiphysics finite element software. Our research adopts a moving coordinate system, a novel approach in this analysis. Specifically, we investigate the effect of different tool rotational speeds (800rpm, 1200rpm, and 1600rpm) while maintaining constant welding speeds (35mm/min) and an axial load of 3kN during the Double-Sided Friction Stir Welding (DFSW) process involving AA 6351-T6 and AA 2024-T351 alloys. For this purpose, the tool material employed is H13 tool steel.

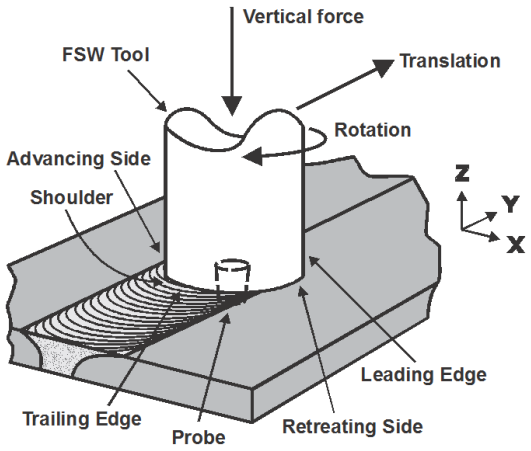

Fig. 1 *FSW process (A. Mishra, 2018)*

Table 1 shows the chemical composition of AA6351-T6 material and table 2 shows the properties of the material AA6351-T6. Table 3 below presents the temperature-dependent material properties of AA6351-T6, with considerations for AA6082-T6 in this analysis (Kasirajan et al. 2019). The variations in specific heat capacity and thermal conductivity at various temperatures are shown in the table. Table 4 shows the chemical composition of the material AA2024-T6. Table 5 shows the properties of the material AA6351-T6.

Table 1 *Chemical composition of the material AA6351-T6*

Component	Si	Fe	Cu	Mn	Mg	Al
%	0.6-1.3	0.6	0.1	0.4-1.0	0.4-1.2	Bal.

Table 2 *AA6351-T6 material properties*

Density	2710 kg/m^3
Modulus of Elasticity	68.9 GPa
Poisson's Ratio	0.33
Coefficient of thermal expansion	23.6e-6 /K

Table 3 *AA6351-T6 / AA6082-T6 temperature dependent properties*

Temperature (K)	353	453	553	653	753	853
Thermal conductivity (W/m K)	162	192	201	217	223	253
Specific heat capacity (J/kg K)	978	1028	1052	1104	1133	1230

Table 4 *Chemical composition of the material AA2024-T6*

Component	Si	Fe	Cu	Mn	Mg	Zn	Al
%	0.046	0.17	4.7	0.65	1.56	0.11	Bal.

Int. Journal of Integrated Engineering Vol. 16 No. 5 (2024) p. 46-55

Table 5 *AA 2024 – T351 material properties*

Density	2780 kg/m^3
Modulus of Elasticity	73.1 GPa
Poisson's Ratio	0.33
Coefficient of thermal expansion	23.2e-6 /K

Table 5 provides the temperature-dependent material properties of AA2024-T351, incorporating the temperature-dependent properties of AA2024-T3 in this analysis (Abdul Wahab H. Khuder et al. 2017). The variations in specific heat capacity and thermal conductivity at various temperatures are shown in the table. Table 6 below provides the chemical composition of the material H13 tool steel. The table 7 below shows the properties of the material H13 tool steel.

Table 5 *Temperature dependent properties of AA2024-T351 / AA2024-T3*

Temperature (K)	293	373	473	573	673	773
Thermal conductivity (W/m K)	164	182	194	202	210	220
Specific heat capacity (J/kg K)	881	927	1047	1130	1210	1300

Table 6 *Chemical composition of H13 tool steel*

Component	C	Mn	Si	P	S	Cr	Mo	Ni	V	Fe
%	0.331	0.321	1.0183	0.014	0.011	5.127	1.0176	0.049	0.989	Bal.

Table 7 *H13 tool steel material properties*

Density	7760 kg/m^3
Specific Heat Capacity	460 J/kg K
Thermal conductivity	24.3 W/m K

2. Mathematical Model

Figure 2 illustrates the model with specified boundary conditions. In the x-direction, two infinite domains are employed on either side of the work piece. Equations (1) to (5) utilized in this study were sourced from the friction stir welding tutorial provided by COMSOL Multiphysics.

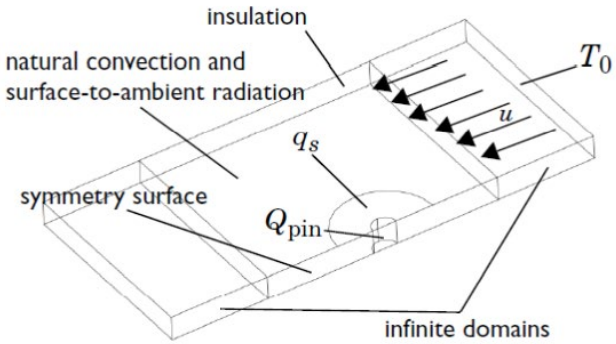

Fig. 2 *FSW COMSOL model with boundary conditions*

Equation (1) governs the heat transfer within the plate.

$$\rho C_p u .\nabla T + \nabla . (-k\nabla T) = Q \quad (1)$$

Here, ρ represents density, C_p denotes specific heat capacity, u signifies velocity, and k stands for thermal conductivity. The heat generated at the interface between the tool pin and the workpiece is expressed by Equation (2).

$$q_{pin}(T) = \frac{\mu}{\sqrt{3(1+\mu)^2}} r_p \omega Y(T) \quad (2)$$

In this context, the variables denote the angular velocity (ω), the friction coefficient (μ), and the pin's radius (r_p). The average shear stress as a function of temperature is also indicated by Y(T). Equation (3) describes the heat

produced at a distance r from the tool centre axis at the interface between the tool shoulder and the plate as a surface heat source.

$$q_{shoulder}(r, T) = \begin{cases} \mu\,(\mathbf{Fn} / \mathbf{As})\,\boldsymbol{\omega}\,\mathbf{r}, & \mathbf{if\ T} < \mathbf{T_{melt}} \\ \mathbf{0}, & \mathbf{if\ T} > \mathbf{T_{melt}} \end{cases} \quad (3)$$

In this equation, F_n represents the normal force acting, A_s represents the surface area of the shoulder, and T_{melt} represents the material's melting point temperature. The heat flux at the upper surface is defined by Equation (4).

$$q_u = h_u (T_o - T) + \epsilon\,\sigma\,(T_a^4 - T^4) \quad (4)$$

The heat flux at the lower surface is defined by Equation (5).

$$q_d = h_d (T_o - T) + \epsilon\,\sigma\,(T_a^4 - T^4) \quad (5)$$

3. Simulation

The simulation study employed COMSOL Multiphysics, a robust finite element analysis software, to analyze temperature distribution during double-sided friction stir welding (DFSW). The analysis involved applying a consistent normal load from a rotating tool at different rotational and welding speeds. The FSW model, depicted in Figure 3, featured two rectangular aluminum alloy plates, AA6351-T6, and AA2024-T351, each sized 100x75x6.3mm. Figure 4 shows the meshing of the model. The simulation parameters, outlined in Table 8, encompassed three distinct rotational speeds (800rpm, 1200rpm, and 1600rpm) while maintaining a constant welding speed of 35mm/min and a vertical normal load of 3kN. The tool, constructed from H13 tool steel, had an 18mm diameter tool shoulder, a 6mm diameter pin, and a tip height of 6.3mm.

The simulation adopted a cylindrical tool pin and applied full constraints on the plate edges to restrict any motion. To facilitate the analysis, various convective boundary conditions were imposed on the plate faces. The heat transfer coefficients were assumed to be 20W/m^{2}K (upside) and 200W/m^{2}K (downside). The mesh details include a maximum element size of 3mm and a minimum element size of 0.03mm, balancing the need for accuracy and computational efficiency. The mesh consisted of a total of 6566 elements. Notably, the model employed a strategic combination of free triangular elements at the pin and shoulder boundaries, optimizing the representation of complex geometries in these critical regions. Simultaneously, a free quad mesh was utilized throughout the remaining areas, enhancing computational efficiency while maintaining a high degree of accuracy in the simulation.

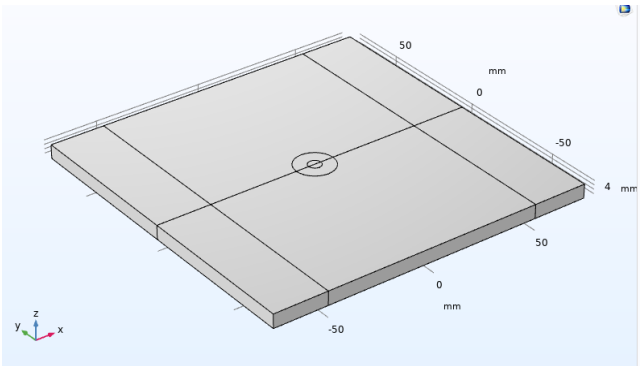

Fig. 3 *Geometry*

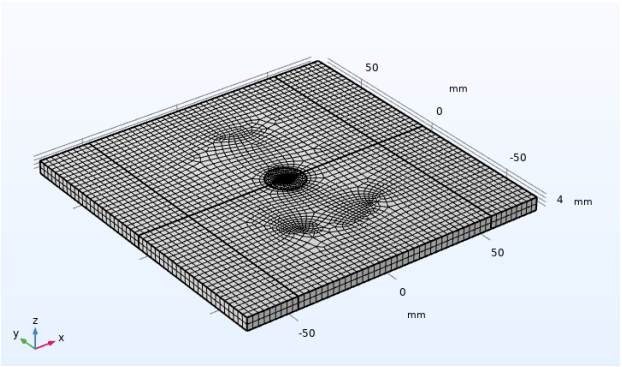

Fig. 4 *Meshing*

Table 8 *Input parameters*

Name	Expression	Value	Description
T0	300[K]	300 K	Ambient temperature
T_melt_6351	922[K]	922 K	Melting temperature of Workpiece_6351
h_upside	20[W/(m^2*K)]	20 W/(m^2·K)	Upper side heat transfer coefficient
h_downside	200[W/(m^2*K)]	200 W/(m^2·K)	Lower side heat transfer coefficient
epsilon	0.3[1]	0.3	Surface emissivity
u_weld	35[mm/min]	5.8333E−4 m/s	Welding speed

Int. Journal of Integrated Engineering Vol. 16 No. 5 (2024) p. 46-55

mu	0.4[1]	0.4	Friction coefficient
n	800[rpm]	13.333 1/s	Rotation speed (RPM)
omega	2*pi[rad]*n	83.776 rad/s	Angular velocity (rad/s)
F_n	3[kN]	3000 N	Normal force
r_pin	3[mm]	0.003 m	Pin radius
r_shoulder	9[mm]	0.009 m	Shoulder radius
A_s	pi*(r_shoulder^2 - r_pin^2)	2.2619E−4 m^2	Shoulder surface area
T_melt_2024	911[K]	911 K	Workpiece_2024 melting temperature

4. Results

The figures 5, 6 and 7 show that the temperature distribution during welding corresponding to different rotational speeds of 800, 1200 and 1600rpm repectively at constant welding speed of 35mm/min and axial load of 3kN. In general, the temperature distribution during FSW can be divided into three zones: the pin zone, the shoulder zone, and the heat-affected zone (HAZ). The pin zone is the region where the rotating tool comes into contact with the materials being welded, and it experiences the highest temperatures during the welding process. The shoulder zone is the region surrounding the pin zone, and it experiences lower temperatures compared to the pin zone. The HAZ is the region surrounding the shoulder zone, and it experiences the lowest temperatures. When welding dissimilar aluminum alloys, the temperature distribution can be affected by differences in the material properties, such as the thermal conductivity and the melting point. The material with higher thermal conductivity will tend to dissipate heat more quickly, resulting in a lower temperature in that region. The material with a higher melting point will require more heat input to reach the plastic state, resulting in a higher temperature in that region. In summary, the temperature distribution in dissimilar FSWed aluminum alloys can vary depending on several factors, including the welding parameters, the tool geometry, and the material properties [Vignesh, R. V. et al. 2016].

However, in general, the pin zone experiences the highest temperatures, followed by the shoulder zone, and the HAZ experiences the lowest temperatures. This can help identify areas of the workpiece that are subjected to high temperatures, which may lead to defects such as voids, cracks, or metallurgical changes. By adjusting the process parameters, such as the tool rotation speed or the welding speed, the temperature distribution can be optimized to achieve a high-quality weld. During FSW, heat is generated due to friction between the rotating tool and the workpiece, and this heat softens the material, allowing it to be welded together [Padmanaban et al. 2014]. However, excessive heat can lead to material defects and poor joint strength. Therefore, temperature distribution analysis is critical to optimize the FSW process. The temperature distribution during FSW of dissimilar materials depends on various factors, such as the tool geometry, tool rotational speed, traverse speed, and material properties. Generally, during the welding process, the temperature at the advancing side of the tool is higher than that at the retreating side. This is because the material is being pushed towards the advancing side and is subjected to more friction and deformation.

The temperature at the joint line is also a critical parameter in FSW. If the temperature is too high, the material may melt and lead to defects such as voids, porosity, and cracking. On the other hand, if the temperature is too low, the material may not be fully consolidated, leading to poor joint strength. The following table 9 shows the maximum temperature obtained from temperature distribution for three different rotational speeds at constant application of the axial load and welding speed. The maximum temperatures of 561K, 679K and 791K were obtained for the rotational speeds of 800rpm, 1200rpm and 1600rpm respectively. The rise in the tool's rotational speed led to a corresponding increase in the maximum temperature in each case. A moving coordinate system was employed in this analysis [Song, M., & Kovacevic, R. 2003]. The below table 9 shows the simulation results at constant welding speed of 35mm/min and an axial load of 3kN.

Table 9 *Simulation results*

S.No.	Rotational speed in rpm	Max.Temp. in K
1	800	561
2	1200	679
3	1600	791

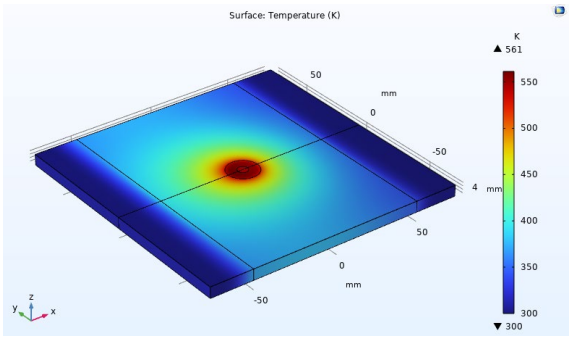

Fig. 5 *Temperature distribution at 800rpm*

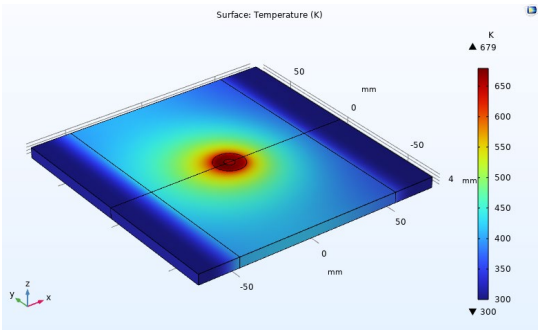

Fig. 6 *Temperature distribution at 1200rpm*

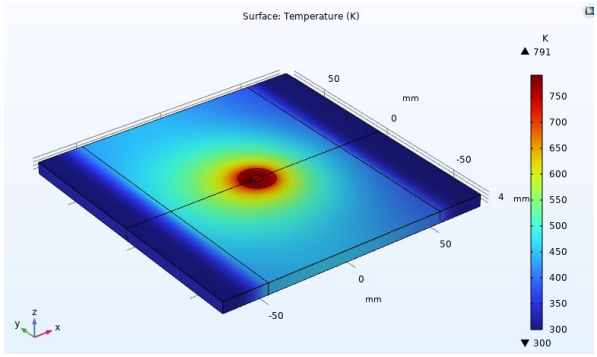

Fig. 7 *Temperature distribution at 1600rpm*

Figure 8 shows that the 2D plot at 800rpm. It represents the various zones like weld nugget zone (red color region) at the centre, the thermo-mechanically affected zone (yellow color region), the heat affected zone (cyan color region) and the unaffected zone (blue color region). The maximum temperature obtained is 557K and the minimum temperature is 373K in this plot. Figure 9 shows that the 2D plot at 1200rpm. The maximum temperature obtained is 673K and the minimum temperature is 409K in this plot. Figure 10 shows that the 2D plot at 1600rpm. The maximum temperature obtained is 783K and the minimum temperature is 443K in this plot.

In dissimilar material welding, the tool encounters different thermal conductivities, heat capacities, melting temperatures, and flow behaviors, resulting in localized temperature variations. The temperature profile typically consists of a highly localized, high-temperature region (the "stir zone") surrounded by a less heated "thermomechanically affected zone" (TMAZ) and a "heat-affected zone" (HAZ) with varying degrees of temperature change. The exact temperature profile will depend on a variety of factors such as the tool geometry, rotational speed, traverse speed, and material properties. The temperature in the stir zone can reach melting or softening temperatures for both materials, resulting in mixing and bonding between the two materials. The TMAZ adjacent to the stir zone experiences significant plastic deformation, with temperature decreasing rapidly away from the stir zone. The HAZ further from the stir zone experiences a smaller temperature increase and little plastic deformation. Figures 11,12 and 13 show that the tempearture graph with respect to the workpiece depth at 800rpm, 1200rpm and 1600rpm respectively. From temperature gradually decreases from the centre of the workpiece to the end of the workpiece on either side.

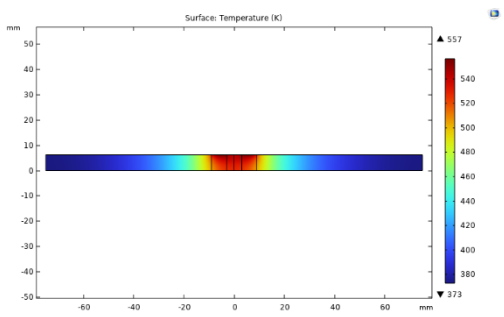

Fig. 8 *2D plot at 800rpm*

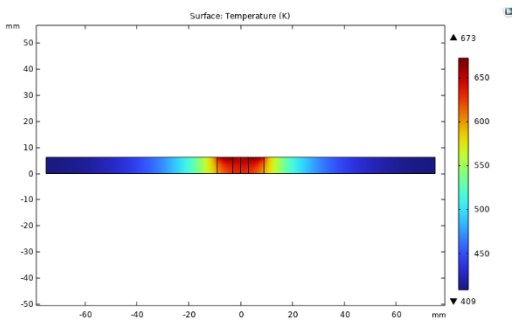

Fig. 9 *2D plot at 1200rpm*

Int. Journal of Integrated Engineering Vol. 16 No. 5 (2024) p. 46-55

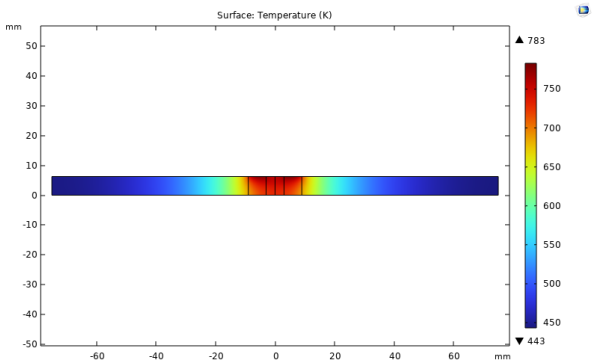

Fig. 10 *2D plot at 1600rpm*

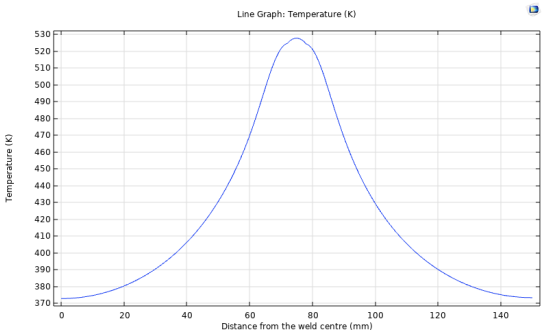

Fig. 11 *1D plot 800rpm*

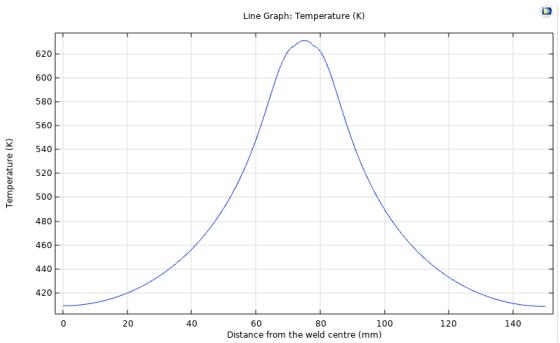

Fig. 12 *1D plot 1200rpm*

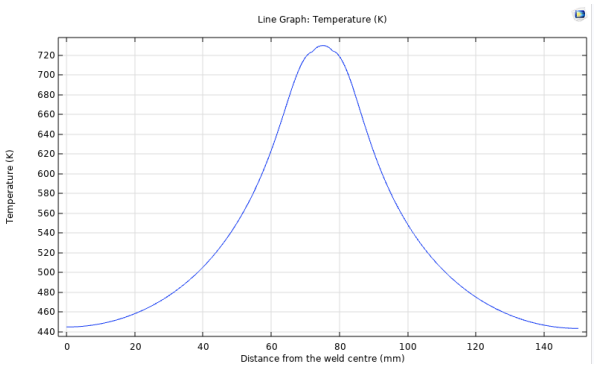

Fig. 13 *1D plot 1600rpm*

5. Experimentation

The FSW setup employed for joining dissimilar aluminum alloys AA2024 and AA6351 involves a robust and precisely controlled apparatus. The FSW machine is equipped with specialized tooling designed to accommodate the dissimilar nature of the alloys. Clamping mechanisms ensure secure fixation of the AA2024 and AA6351 plates, facilitating consistent material flow during welding. The tool, featuring a threaded shoulder and a tapered pin with a wear-resistant material, is configured to provide the necessary rotational and axial forces. Real-time monitoring and feedback systems ensure accurate control of welding parameters, including rotation speed, welding speed, and axial force. This setup ensures the generation of defect-minimized, high-quality joints between dissimilar aluminum alloys, enabling comprehensive investigations into joint properties and microstructural characteristics. Figure14 illustrates the secure fixation of samples on the FSW machine (Available at JNTUK. AP), ensuring proper alignment. Figure 15 shows the FSW cylindrical tool made of H13 tool steel, with a pin diameter of 6mm and a depth of 6mm. Table 10 below shows the specifications of the FSW machine 3T-NC available at JNTUK. Figures 16 to 18 illustrate the resulting FSW welds at three distinct speeds: 800rpm, 1200rpm, and 1600rpm, all executed at a welding speed of 35mm/min and an axial force of 3kN.

Fig. 14 *Plates fixed on the machine*

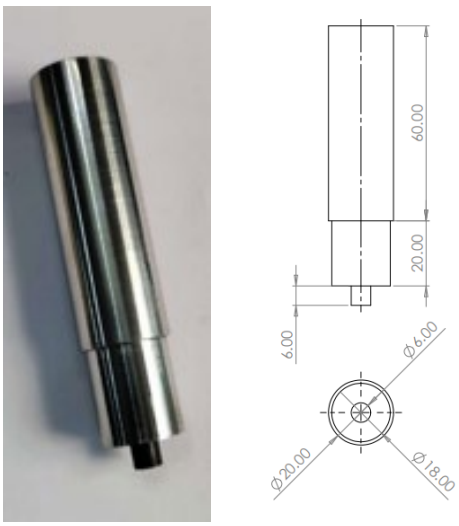

Fig. 15 *FSW Cylindrical tool*

Table 10 *FSW specifications*

Spindle	ISO40
Spindle Motor	AC Induction Motor
Z-Axis Stroke	300mm, Thrust- 30kN, Drive- Servo Motor
X-Axis Stroke	400mm, Thrust- 15kN, Drive- Servo Motor
Y-Axis Stroke	200mm, Drive- Manual
Centralized Lubrication System (Manual)	
NC Force Control & Position Control	

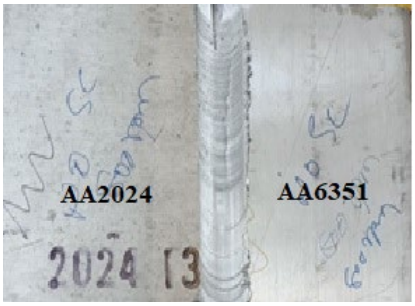

Fig. 16 *FSW at 800rpm*

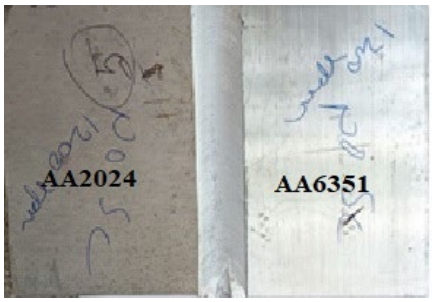

Fig. 17 *FSW at 1200rpm*

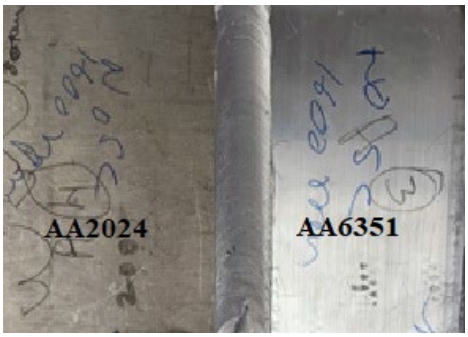

Fig. 18 *FSW at 1600rpm*

6. Validation

The maximum temperature is recorded while doing the experiment using Infrared industrial thermometer of model HTC IRX 68 and the temperature range of which is −50 to1850°C. These were validated with the numerical results, and they were in a good agreement. The table 11 below shows the values of maximum temperature obtained both in simulation and experimentation and they were in good agreement. Figure 19 shows that the

Int. Journal of Integrated Engineering Vol. 16 No. 5 (2024) p. 46-55

graph between Maximum Temperature and Rotational Speed during simulation and experimental analysis. At 800 rpm, the simulated maximum temperature was 288°C, while the experimental temperature recorded using the infrared thermometer was 279°C. This relatively small discrepancy of 9°C suggests a consistent and accurate performance of the HTC IRX 68 in capturing temperatures during FSW at lower rotational speeds. Similarly, at 1200 rpm, the simulated temperature reached 406°C, while the experimental measurement yielded 390.4°C. The proximity of these values (within approximately 15.6°C) further validates the reliability of the infrared thermometer across a broader range of temperatures and welding conditions.

At the highest rotational speed of 1600 rpm, the simulated temperature was 518°C, closely aligning with the experimentally measured temperature of 509°C. This agreement highlights the thermometer's robustness in accurately capturing temperatures even under more challenging and dynamic welding conditions. The observed consistency between the simulated and experimental temperature data supports the validation of the HTC IRX 68 infrared thermometer for measuring temperatures during FSW. The small variations in temperature readings can be attributed to factors such as heat dissipation, thermal conductivity, and specific material properties, which may not be fully captured by simulation models.

Table 11 *Maximum temperature values in both simulation and experimentation*

Rotational speed in rpm	Max. Temp. in °C (Simulation)	Max. Temp. in °C (Experimentation)
800	288	279
1200	406	390.4
1600	518	509

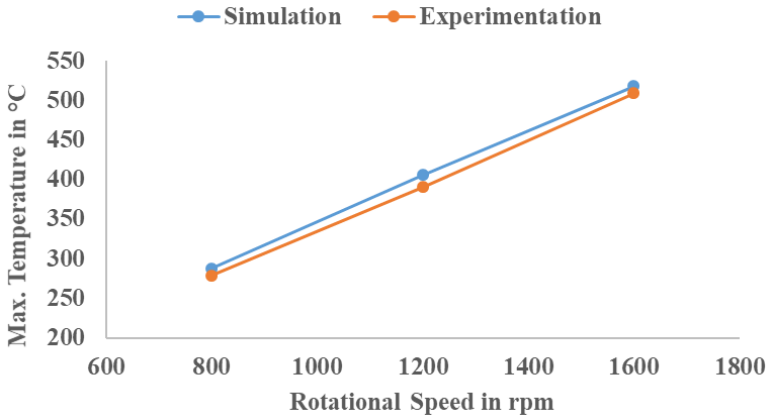

Fig. 19 *Experimental validation of maximum temperature*

7. Conclusions

In the culmination of the study, the Friction Stir Welding (FSW) procedure demonstrated effective amalgamation of dissimilar Aluminum alloy materials, specifically AA6351-T6 and AA2024-T351, while ensuring a consistent axial load throughout the analysis. The successful execution of numerical analysis, facilitated by COMSOL Multiphysics software, provided a comprehensive understanding of the welding process. Notably, an escalation in maximum temperature was observed with an increase in the tool's rotational speed. Both simulation and experimentation recorded maximum temperatures of 518°C and 509°C at a rotational speed of 1600rpm, maintaining a constant welding speed of 35mm/min and an axial force of 3kN. Importantly, these temperatures remained below the melting point of the workpieces, underscoring the robustness of the chosen parameters. The thermal analysis outcomes offer crucial insights for process optimization, aiding in the determination of optimal welding parameters, tool design, and the formulation of strategies for post-welding heat treatment. This comprehensive approach enhances the overall understanding of dissimilar alloy welding, contributing to advancements in material joining techniques.

Acknowledgement

The authors extend their sincere gratitude to the Department of Mechanical Engineering, Andhra University, for providing the essential support and resources crucial for the successful execution of this research. Additionally, heartfelt thanks are extended to JNTU Kakinada for granting permission to conduct Friction Stir Welding (FSW) experimentation using the FSW machine, thereby enabling the practical validation of our study.

Conflict of Interest

The authors declare that there is no conflict of interest.

Author Contribution

The authors confirm contribution to the paper as follows: ***study conception and design:*** *K. Samadhanam Raju, N. Ramanaiah;* ***data collection:*** *K. Samadhanam Raju;* ***analysis and interpretation of results:*** *K. Samadhanam Raju, N. Ramanaiah;* ***draft manuscript preparation:*** *K. Samadhanam Raju. All authors reviewed the results and approved the final version of the manuscript.*

References

[1] Thomas, W. M., Nicholas, E. D., Needham, J. C., Murch, M. G., Templesmith, P., & Dawes, C. J. (1991). GB Patent application no. 9125978.8. *International patent application no. PCT/GB92/02203*.

[2] Song, M., & Kovacevic, R. (2003). Thermal modeling of friction stir welding in a moving coordinate system and its validation. *International Journal of machine tools and manufacture*, *43*(6), 605-615.

[3] Zhang, Z., & Zhang, H. W. (2009). Numerical studies on the effect of transverse speed in friction stir welding. *Materials & Design*, *30*(3), 900-907.

[4] Padmanaban, R. V. R. K., Kishore, V. R., & Balusamy, V. (2014). Numerical simulation of temperature distribution and material flow during friction stir welding of dissimilar aluminum alloys. *Procedia Engineering*, *97*, 854-863.

[5] Salimi, S., Bahemmat, P., & Haghpanahi, M. (2014). A 3D transient analytical solution to the temperature field during dissimilar welding processes. *International Journal of Mechanical Sciences*, *79*, 66-74.

[6] Vignesh, R. V., Padmanaban, R., Arivarasu, M., Thirumalini, S., Gokulachandran, J., & Ram, M. S. S. S. (2016, September). Numerical modelling of thermal phenomenon in friction stir welding of aluminum plates. In *IOP conference series: materials science and engineering* (Vol. 149, No. 1, p. 012208). IOP Publishing.

[7] Maharia, A. K., Sahu, S., & Ansari, M. Z. (2018, August). Temperature and thermal stress distribution in underwater friction stir welding of aluminium plates. In *IOP Conference Series: Materials Science and Engineering* (Vol. 404, No. 1, p. 012034). IOP Publishing.

[8] Pamuk, M. T., Savaş, A., Seçgin, Ö., & Arda, E. (2018). Numerical simulation of transient heat transfer in friction-stir welding. *International Journal on Heat and Technology*.

[9] Tayo, O. A., Laseinde, T. O., & Mashinini, M. Finite-Element modeling of Thermo-Mechanical phenomena in friction stir welding of AISI 4340 steel.

[10] Vishwanath, M. M., Lakshamanaswamy, N., & Ramesh, G. K. (2019). Numerical Simulation of Heat Transfer Behavior of Dissimilar AA5052-AA6061 Plates in Fiction Stir Welding: An Experimental Validation. *Strojn cky asopis-Journal of Mechanical Engineering*, *69*(1), 131-142.

[11] Sevvel, P., Babu, S. D., & Kumar, R. S. (2020). Peak Temperature Correlation and Temperature Distribution during Joining of AZ80A Mg Alloy by FSW-A Numerical and Experimental Investigation. *Journal of Mechanical Engineering/Strojniški Vestnik*, *66*(6).

[12] Lemi, M., Gutema, E., & Gopal, M. (2022). Modeling and simulation of friction stir welding process for AA6061-T6 aluminum alloy using finite element method. *Engineering Solid Mechanics*, *10*(2), 139-152.

[13] Kasirajan, T., Ravindran, R., Ramkumar, T., & Selvakumar, M. (2019). Investigation of the microstructural, mechanical, and thermal evolution of dissimilar aluminium alloys during friction stir welding. *Transactions of the Canadian Society for Mechanical Engineering*, *44*(1), 38-48.

[14] Khuder, A. W. H., Muhammed, M. A., & Ibrahim, H. K. (2017). Numerical and experimental study of temperature distribution in friction stir spot welding of AA2024-T3 Aluminum Alloy. *Int. J. Innov. Res. Sci. Eng. Technol*, *6*, 1111-1121.

[15] Mishra, A. (2018). Friction stir welding of dissimilar metal: a review. *Available at SSRN 3104223*.

[16] A tutorial on Friction Stir Welding of an Aluminum Plate created in COMSOL Multiphysics 6.1. https://doc.comsol.com/6.0/doc/com.comsol.help.models.heat.friction_stir_welding/models.heat.friction_stir_welding.pdf